Dissimilar Dynamics of Coupled Water Vibrations

Thomas l. C. Jansen, Dan Cringus, and Maxim S. Pshenichnikov*

Zernike Institute for Advanced Materials, University of Groningen, Nijenborgh 4, 9747 AG Groningen, The Netherlands

Received: January 16, 2009; Revised Manuscript Received: March 25, 2009

Dissimilar dynamics of coupled stretch vibrations of a water molecule are revealed by two-dimensional IR correlation spectroscopy. These are caused by essentially non-Gaussian fluctuations of the electric field exerted by the environment on the individual OH stretch vibrations. Non-Gaussian statistics of the individual site frequency fluctuations results in distinctively different dephasing of the symmetric and asymmetric eigenmodes. This phenomenon can only be described if the assumption of Gaussian dynamics in the traditional theories is abandoned.

Introduction

The importance of solvation and, more generally, dynamical processes in liquids can hardly be exaggerated as they play a crucial role in chemistry, biology, and physics.[1,2] Therefore, it is not surprising that in the last decades much effort has been devoted—both theoretically and experimentally—to the understanding of solvation processes and dynamics. Ultrafast optical spectroscopy has proven to be one of the most successful tools in revealing solvent dynamics from such observables as (non)linear optical spectra.[3] For the study of solvation, a single chromophore decoupled from any other chromophore of its kind is usually considered. However, the situation where a chromophore is isolated is not always possible, desired, or even realistic. In complex molecular systems that contain multiple chromophores, such as light-harvesting complexes,[4] proteins,[5] molecular aggregates,[6,7] dendrimers,[8,9] polymers,[10] and any bulk liquid,[11−14] couplings between the local modes result in the formation of delocalized eigenmodes which become new spectroscopic observables. Conventional theories[3] that assume frequency dynamics to obey Gaussian statistics[15] predict no differences in dynamics between local and eigenmodes as was convincingly demonstrated by Tokmakoff and co-workers on a model acetylacetonato−dicarbonyl rhodium (RDC) system.[16] However, the fundamental question remains whether these assumptions are valid for more realistic cases.

We will illustrate the above outlined general ideas by a simple yet insightful example (Figure 1a). Let us consider two identical, coupled two-level systems as a model for the symmetric (s) and asymmetric (a) modes, with fluctuating site frequencies $\omega_1(t)$ and $\omega_2(t)$ ($\langle\omega_1(t)\rangle = \langle\omega_2(t)\rangle = \omega_0$, where the brackets denote time-averaging). Any optical spectroscopy is sensitive to the eigenfrequencies, which are[17]

$$\omega_{a,s}(t) = \frac{\omega_1(t) + \omega_2(t)}{2} \pm \frac{1}{2}\sqrt{4J^2(t) + [\omega_1(t) - \omega_2(t)]^2} \tag{1}$$

where $J(t)$ stands for the time-dependent coupling. The dynamics of the eigenmodes are governed by the two-point frequency−frequency correlation functions[3] (CFs) $S_s(t) = \langle\omega_s(0)\cdot\omega_s(t)\rangle$ and $S_a(t) = \langle\omega_a(0)\cdot\omega_a(t)\rangle$ for the frequencies of symmetric and asymmetric modes, respectively. One possibility for eigenmodes dynamics to be different is that the fluctuating coupling is correlated with the site frequency. This becomes more apparent if one considers the approximation of strong coupling, i.e., $|J(t)| \gg |\delta\omega|$, where $\delta\omega$ is the rms amplitude of frequency fluctuations:

$$S_{a,s}(t) \cong \frac{1}{2}\langle\omega_1(0)\cdot\omega_1(t)\rangle + \frac{1}{2}\langle\omega_1(0)\cdot\omega_2(t)\rangle + \langle J(0)\cdot J(t)\rangle \pm \langle\omega_1(0)\cdot J(t)\rangle \tag{2}$$

It is the last term in eq 2 that apparently gives rise to the CF differences. For instance, in the case of vibrational modes, the coupling originates from changes in the electron density caused by one vibrational mode to nuclear coordinates at the other site. Therefore, modulation of the local electron density by environmental fluctuations could result—at least, hypothetically—in correlation between the site frequency and coupling. It is also seen from eq 2 that when the coupling fluctuations are weak and the site frequencies are uncorrelated, the amplitude of the CF is by a factor of 2 lower than in the uncoupled case due to the effect of exchange narrowing.[18]

The alternative (or complementary) possibility would be that the coupling is weakly fluctuating while there exists a correlation between the first fraction and square-root terms in eq 1. This could be readily seen assuming $J(t) = \text{const}$ and expanding the square-root term in eq 1 into the Taylor series

$$S_{a,s}(t) \cong \frac{\langle\omega_1(0)\cdot\omega_1(t)\rangle + \langle\omega_1(0)\cdot\omega_2(t)\rangle}{2} \pm \frac{\langle\omega_1(0)\cdot\omega_1^2(t)\rangle + \langle\omega_1(0)\cdot\omega_2^2(t)\rangle - 2\langle\omega_1(0)\cdot\omega_2(0)\cdot\omega_1(t)\rangle}{8|J|} \tag{3}$$

where the higher-order terms were omitted. Getting different dynamics of the two modes in this case requires the odd-order CFs such as $\langle\omega_1(0)\cdot\omega_1^2(t)\rangle$ to be nonzero or, in other words, the site frequency dynamics to be essentially non-Gaussian (because for the Gaussian dynamics the odd-order CFs are zero[15]). In either case, the ability to obtain differences in the dynamics would tremendously enrich our knowledge of solvation behavior.

* To whom correspondence should be addressed. E-mail: M.S.Pchenitchnikov@RuG.nl.

10.1021/jp900480r CCC: $40.75
Published on Web 05/13/2009

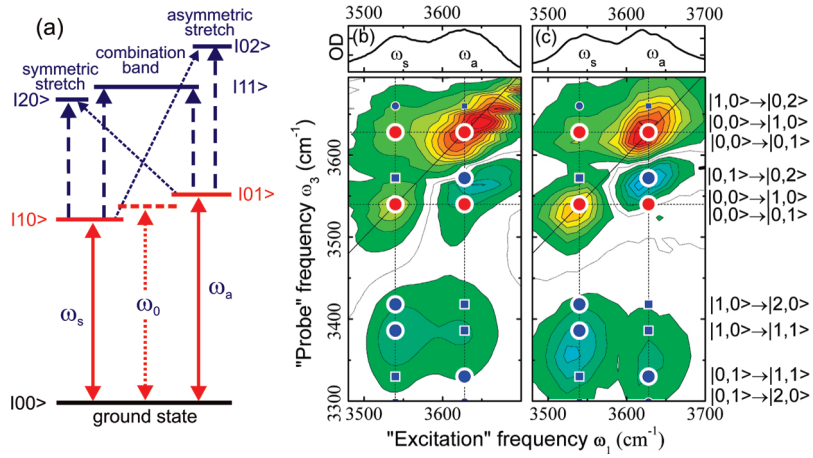

Figure 1. (a) Energy level diagram showing the transitions relevant to the experiments. The notation |sa> stands for the quantum numbers associated with the symmetric and asymmetric stretch of the H−O−H molecule, respectively. Frequency ω_0 corresponds to the site frequency of the (uncoupled) OH stretches, while coupling J gives rise to splitting into symmetric (frequency ω_s) and asymmetric (frequency ω_a) modes separated by $2J$. (b, c) 1D (top panels) and 2D (low panels) absorptive spectra of H_2O in acetonitrile in the OH stretching region. The experimental (b) and calculated (c) spectra are shown for a 0 fs waiting time. The maximum (red) and minimum (blue) of the signal are separated by equally spaced levels (10% of the maximum), while the dotted curve corresponds to zero amplitude. The circles depict the positions of the direct transitions (assigned in the right) as depicted in (a), while squares stand for coherent and/or population transfer contributions to the 2D spectrum.

However, the conventional steady-state absorption spectroscopy yields a time-averaged projection of fluctuating frequencies rather than a CF.[3] To get a hold of the latter, one has to bring into play the second frequency dimension as provided by two-dimensional (2D) correlation spectroscopy.[19−22]

2D IR spectroscopy has been shown to be capable of revealing the finest details of transient molecular dynamics that are otherwise hidden beneath broad featureless absorption bands.[20−22] A few well-documented examples of additional information contained in the 2D spectra include—but are not limited to—the coupling between different vibrations resulting in cross-peaks,[23] correlation between fluctuations of the environment near different vibrations affecting the tilt of the cross-peaks,[16] and the environmental dynamics obtained from changes in the shapes of diagonal peaks.[24]

Here we show that coupling together with non-Gaussian statistics of frequency fluctuations of the individual OH stretch of a water molecule results in distinctively different dynamics of the symmetric and asymmetric eigenmodes. A comprehensive theoretical analysis based on combined MD−quantum mechanical simulations identifies the underlying physical processes accountable for such dissimilarity. Our results demonstrate that at least for hydrogen bonding systems a paradigm shift is needed: conventional spectroscopic theories[3] ought to be complemented with computational methods that combine molecular dynamics, electronic structure calculations, and solving the time-dependent Schrödinger equation for the vibrational degrees of freedom. In particular, our findings are highly relevant for a better understanding of the dynamics of complex systems such as proteins, polymers, and light-harvesting complexes.

Experimental Section

As a model system, we chose a water molecule diluted in acetonitrile at room temperature. In this system, two OH vibrations are coupled via the oxygen atom while intermolecular water−water interactions are reduced to naught by use of an extremely low water concentration (molar ratio < 0.02).

The 2D spectra were measured following the nowadays standard protocol.[21] In brief, 70 fs, 3 μm IR pulses from a home-built optical parametric amplifier were split into two pairs. The first pair of pulses separated by t_{12} imprints a frequency-modulated population grating[24] that is allowed to propagate for the evolution time t_{23}. During this time, the environmental fluctuations tend to wash out the grating: the finer the grating is, the more catastrophic is the loss of memory for the initial frequency modulation. The third pulse is scattered off the remaining grating and heterodyned by the fourth pulse at an MCT array producing the spectrum along the "probe" ω_3 axis. The Fourier transformation of the obtained pattern over the t_{12} time to the "excitation" frequency domain ω_1 results in the 2D correlation spectra.

The excitation pulse energies were kept as low as ~2 μJ, while the heterodyned pulse was about 100 times weaker. All beams were focused to the spot of 100 μm diameter at the sample that was contained in a 50 μm thick, free-standing jet. Under such experimental conditions, the fraction of excited water molecules did not exceed 1%, which makes the higher-order nonlinear processes improbable. Experiments performed on neat acetonitrile revealed no substantial nonresonant solvent contribution.

Results and Discussion

The FTIR absorption spectrum of water diluted in acetonitrile sample (Figure 1b, upper panel) clearly demonstrates splitting of the coupled OH stretches into the higher-frequency asymmetric (at 3630 cm^{-1}) and lower-frequency symmetric (at 3540 cm^{-1}) modes. Note that strictly speaking, this designation is not entirely appropriate because the modes average participation ratio of 1.5 lies between the values of 1 and 2 for the fully localized and delocalized modes, respectively.[25] The mixed mode character arises because the average coupling ($\langle J(t)\rangle = -43.8$ cm^{-1}, vide infra) is comparable to the rms width of the site frequency distribution (~62 cm^{-1}). Nonetheless, for the sake of simplicity we will use the terminology as if the modes were delocalized.

An example of the 2D spectrum at evolution time $t_{23} = 0$ is shown in Figure 1b. The energy level diagram for the molecule (Figure 1a) fully explains the peak positions. Two peaks at ~3540 and ~3630 cm^{-1} correspond to the symmetric and asymmetric stretching OH vibrations, respectively (Figure 1a). The cross-peak at ω_1~3540 and ω_3 ~ 3630 cm^{-1} is already visible at an early waiting time which indicates that these two

modes share the same ground state. The second cross-peak at $\omega_1 \sim 3630$ and $\omega_3 \sim 3540$ cm^{-1} is suppressed because of its coincidental overlap with the excited state absorption at $\omega_3 \sim 3560$ cm^{-1} by the asymmetric stretch (blue contours). At lower values of ω_3 additional excited states absorption peaks are observed in accordance with the energy level diagram. While these peaks contain additional information on, for instance, anisotropy,[26] its encoding is rather difficult due to substantial broadening, mixed symmetry, and dynamics of the respective transitions. For this reason, here we will mainly focus on the analysis of diagonal peaks retaining the excited state transitions as a general proof of the adequacy of the theoretical modeling.

The correlation spectra obtained at different evolution times t_{23} (i.e., delays between the pulse pairs) are shown in Figure 2a. At zero delay, both diagonal peaks are diagonally elongated, which is indicative of inhomogeneous broadening of the symmetric and asymmetric modes. However, the homogeneous contribution to the symmetric mode seems to exceed that for the asymmetric mode. This becomes more apparent at the longest evolution times where the asymmetric mode response still carries some inhomogeneity while the symmetric one has almost round shape, and, therefore, its initial inhomogeneity has vanished.

To quantify these observations and facilitate further comparison with simulations, we extended the line-shape analysis presented in ref 24 to account for multiple transitions in a 2D spectrum as follows.[27,28] Each cut at frequency ω_1 through a 2D spectrum was fitted with a combination of three Gaussians from which the positions of the maxima were found (Figure 2a). The slope of the curve connecting the maxima can be regarded as an indicator for the amount of dephasing at the given frequency.[27] For a fully correlated response (for instance, at short waiting times), this slope is 1, and for uncorrelated—zero. In the case of Gaussian dynamics, the slope value is exactly equal to the normalized to unity CF at the evolution time t_{23}.[24] Additional benefits of such analysis originate from the following factors: first, the slope values are not sensitive to the particular spectra normalization, and second, the method produces the dimensionless quantities which are very suitable for direct comparison.

Figure 3 summarizes this slope analysis by showing the respective slopes averaged about the frequencies of symmetric and asymmetric modes. It convincingly confirms that the symmetric mode dephases much quicker than the asymmetric one, at all evolution times. Different dephasing times could not be predicted by a standard theory (like, for instance, the multimode Brownian oscillator model[3]) where both modes sample similar environmental dynamics.

To assist the interpretation of the experimental results, we performed combined MD and quantum mechanical simulations in the following way. First, the GROMACS 3.1.4[29] program was run using the acetonitrile force field developed by Guardia et al.[30] and the standard SPC/E[31] force field for water. For both molecules, the bond lengths and angles were kept fixed. We used a box containing 1 water molecule and 296 acetonitrile molecules. A 1 ns trajectory was produced using 1 fs time steps, while the snapshots were saved every 10 fs. Second, the OH stretch frequencies, coupling, and transition dipole moments were extracted from the MD trajectory using a recently published electrostatic ab initio map.[32] This map includes the solvent-induced polarization of the transition dipoles (the non-Condon effect), which was demonstrated to be crucial for a correct description of the OH stretch spectrum.[33] The linear

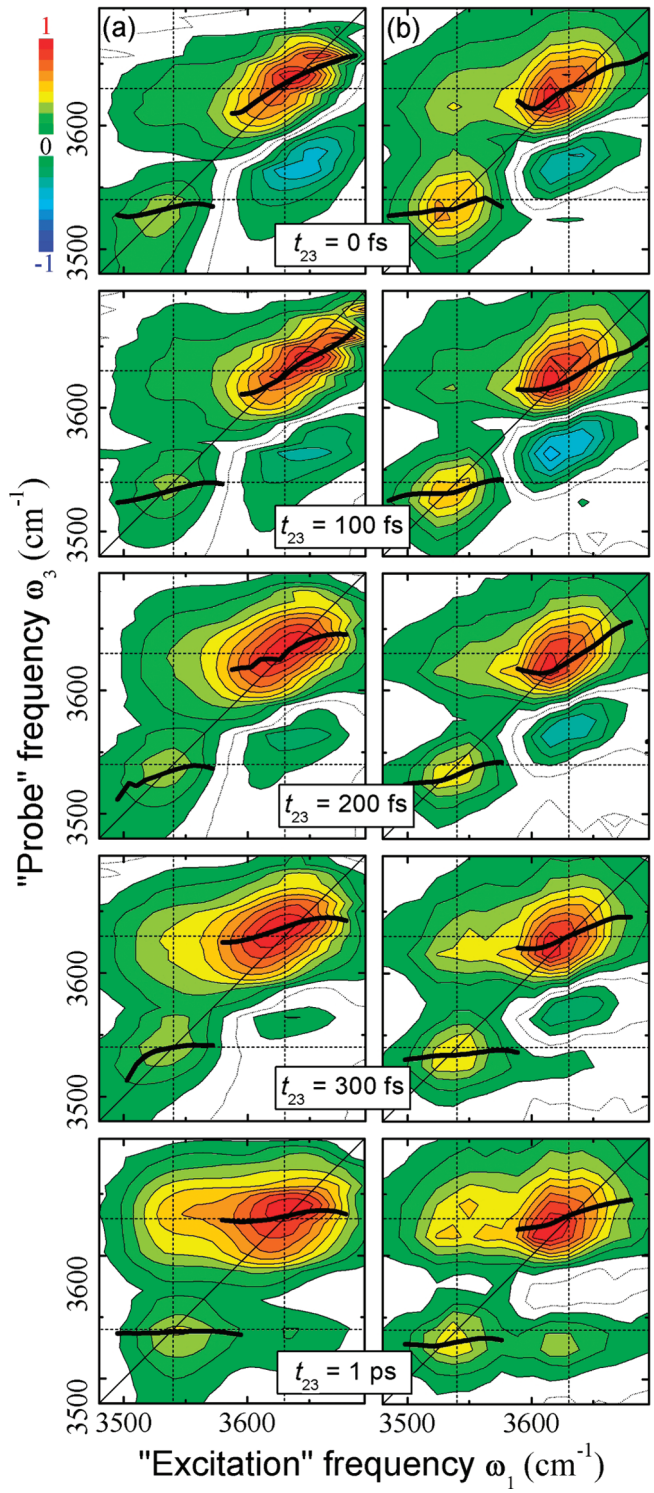

Figure 2. 2D absorption spectra at different evolution times t_{23}. Left (a) and right (b) columns present experimental and simulated data, respectively. Polarizations of all pulses are linear and identical. Dotted lines show frequencies of symmetric and asymmetric stretching modes of the H_2O molecule. The 2D spectra are normalized to the maximal amplitude. The isocontours are drawn at 10% steps of the maximal amplitude. Solid black curves connect maxima at the given excitation frequency ω_1.

absorption IR and Raman spectra of bulk water were excellently reproduced with this map.[34] For direct comparison with experiment, the site frequencies were shifted 35 cm^{-1} to the red. Finally, a standard fluctuating vibrational Hamiltonian was constructed with these parameters

$$H(t) = \omega_1(t)B_1^+B_1 + \omega_2(t)B_2^+B_2 + J(t)(B_1^+B_2 + B_2^+B_1) - \frac{\Delta}{2}(B_1^+B_1^+B_1B_1 + B_2^+B_2^+B_2B_2) \quad (4)$$

where B^+ and B stand for Bose creation and annihilation operators, respectively. A constant anharmonicity value of $\Delta = 210$ cm^{-1} for the isolated OH stretch vibrations[26] was added to the Hamiltonian to account for the doubly excited states. The linear absorption and 2D-IR spectra were simulated with the numerical integration of the Schrödinger equation scheme[35] using the Hamiltonian (eq 3). This method directly calculates the response function from the MD trajectories and automatically accounts for non-Gaussian effects if present even in the extreme case of chemical exchange.[36] Note that the so-called coherent pathways,[37] i.e., when the light−matter interaction proceeds via a coherent superposition of symmetric and asymmetric modes during the waiting time, are automatically included in the simulations despite their relatively low contribution.

The simulated linear spectrum (Figure 1c, upper panel) reproduces the experimental one (Figure 1b) quite well given the fact that *no free parameters were used.* The simulated 2D spectra (Figures 1c and 2b) are also in good agreement with the experimental observations (Figures 1b and 2a). This also holds for the slope values of the calculated 2D patterns (Figure 2b, black curves), which fall excellently on the experimental data (Figure 3). The calculated CF of the asymmetric mode decays indeed much slower than the symmetric one (Figure 4a), which is fully consistent with the slope analysis. The latter has been proven[24] to yield the right values of the CF only for Gaussian fluctuations, whereas the non-Gaussian case has never been considered theoretically as yet. Our results suggest that applicability of the method seems to be broader than was originally thought, at least for systems with a moderate contribution of non-Gaussian dynamics. The discrepancy between the slope analysis and CFs observed at very short times is caused by the breakdown of approximations used in the theoretical analysis.[24]

Now the question is from where the difference between the CFs of the symmetric and asymmetric modes originates. To answer this question, we analyzed the individual CFs obtained from the simulations (Figure 4b). The OH site frequency CF $\langle\omega_1(0)\cdot\omega_1(t)\rangle$ (solid blue curve) first decays on the time scale of ∼50 fs which, after a recurrence at ∼200 fs, is followed by a longer, 1.5 ps decay. To identify the underlying molecular processes, we examined the mutual configurations and motions of water and acetonitrile molecules at different times. The 50 fs initial decay is caused by strongly damped librations of the water molecule about the mean frequency of ∼650 cm^{-1} reported earlier.[38] The recurrence at ∼200 fs observed also in the experimental slope (Figure 3) is due to underdamped low-frequency intermolecular hydrogen bond stretching modes. This was verified by calculating the correlation function of the shortest H···N distance, which shows the same recurrence at ∼200 fs (Figure 5). These results are in line with general findings by others for an HDO molecule dissolved in D_2O.[33,39,40]

The standard deviation of the coupling fluctuation about the average coupling value of $\langle J(t)\rangle = -43.8$ cm^{-1} is only 4.2 cm^{-1}. For this reason, the CF of the coupling $\langle J(0)\cdot J(t)\rangle$ is so small (Figure 4b, dotted line) that its contribution can be safely disregarded. Quite unexpectedly for us, the cross-correlation between the fluctuating coupling and site frequency $\langle\omega_1(0)\cdot J(t)\rangle$

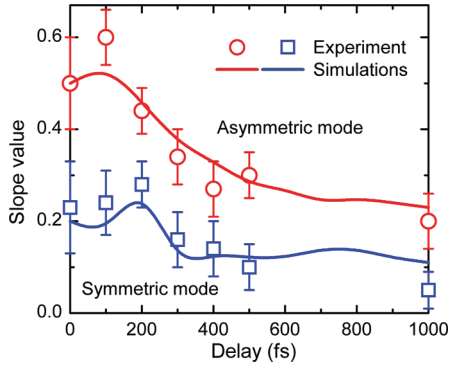

Figure 3. Results of the slope analysis of the experimental (symbols) and simulated (curves) 2D spectra for the asymmetric (red circles and red curve) and symmetric (blue squares and blue curve) stretching mode.

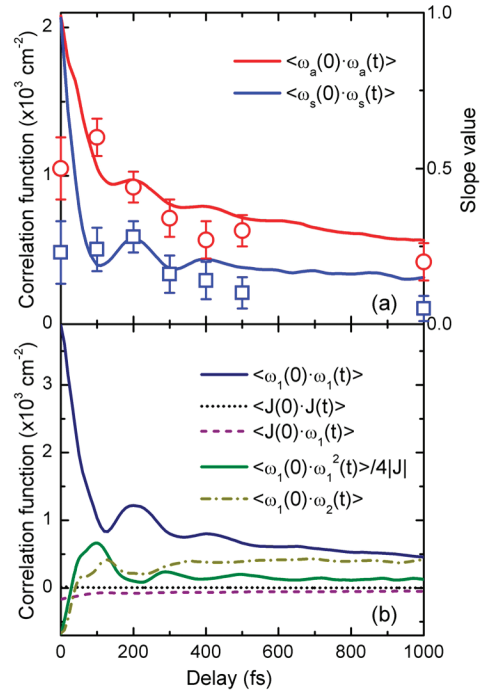

Figure 4. (a) CFs of the asymmetric (red curve) and symmetric (blue curve) stretching mode obtained from computer simulations, superimposed with the results of the slope analysis of the experimental 2D spectra (symbols). (b) Calculated site frequency CF (solid blue), site frequencies cross-CF (dash-dotted), coupling CF (dotted), site frequency-coupling cross-CF (dashed), and third-order site frequency CF (solid green).

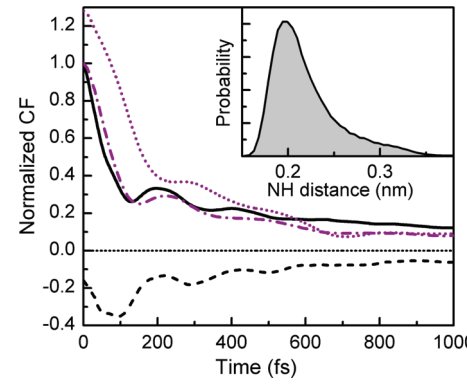

Figure 5. CFs of the electric field exerted on each hydrogen atom by the closest neighboring nitrogen atom (solid curve, second-order CF; dashed curve, third-order CF), and the hydrogen bond distance N···H (dash-dotted curve, second-order CF; dotted curve, third-order CF). Inset: distribution of the hydrogen bond distances.

(dashed curve) is *not sufficient* to account for differences between the symmetric and asymmetric mode CFs (consult eq 2), thereby revoking the first scenario outlined in the Introduction. Therefore, we focused on correlations between the first fraction and square-root terms in eq 1 and found that odd-order CFs like, for instance, $\langle \omega_1(0) \cdot \omega_1^2(t) \rangle$, are not vanishing (solid green curve) as they do for a Gaussian random process.[15] The plus/minus sign in eq 3 results in dissimilar dynamics of the asymmetric/symmetric modes and, in particular, is accountable for suppressing/enhancing the recurrence at 200 fs (Figure 4a) that is also apparent in the third-order CF but has a 180° phase shift with respect to CFs. The slope value analysis of the experimental data seems to support this conclusion but at the edge of its accuracy. The third-order site frequency cross-CFs (like $\langle \omega_1(0) \cdot \omega_2^2(t) \rangle$) are about 1 order of magnitude smaller than the ones involving only one site, and as such they have little importance for the understanding of the dynamics.

We note that, as follows from eq 1, had the site frequency fluctuations been fully correlated, the two peaks would have exhibited identical dynamics. In this respect, it is instructive to calculate the cross-CF between the two site frequencies (Figure 4b, dash-dotted curve). It starts at ~17% of the value of the site frequency CFs and is negative at short times (i.e., the OH site frequencies are partly anticorrelated). The cross-CF turns positive after ~50 fs and reaches the site frequency CF by 1 ps, when molecular motions become more collective, and therefore differences between the two hydroxyl groups dynamics vanish. The initial anticorrelation of the site frequencies also explains the absence of quantum beats (with a period of ~370 fs) in the slope values that are characteristic of coherent excitation of frequency-*correlated* transitions.[41,24,42,43]

As a final test, we computer-generated the frequency trajectories with the same amplitude rms deviations but having strictly Gaussian statistics and uncorrelated site frequencies. Indeed, their substitution instead of those obtained from the genuine MD simulations resulted in identical dynamics for the symmetric and asymmetric modes and the appearance of the quantum beats at ~350 fs.

Having established the non-Gaussian character of the site frequency dynamics, we can trace its origin from the simulations. For that, we analyzed the higher-order CFs of the electric field generated by the solvent along the OH bond, and the hydrogen bond distance (H···N). The vibrational frequency is a quadratic function of the electrical field,[32] and the modulation of the hydrogen bond distance is expected to give a major contribution to the electric field fluctuations.[32,39,44] The second- and third-order CFs were calculated for these quantities and normalized by dividing with the standard deviation to the second- and third-order, respectively (Figure 5). The second- and third-order CFs of the electric field closely resemble those for the site frequency fluctuations (Figure 4b). However, the normalized third-order CF of the hydrogen bond coordinate is significantly larger than that of the electric field. This demonstrates that the underlying molecular dynamics are even more non-Gaussian in character than the electric field or/and the frequency fluctuations. This is highlighted in the inset of Figure 5 where a long non-Gaussian tail is evident in the distribution of the hydrogen bond distances. The inverse distance squared dependence of the electric field—which ultimately defines the OH site frequency—compresses this tail but not enough for suppressing non-Gaussian statistics of the frequency fluctuations.

With the success of describing heterogeneous dynamics in the acetonitrile−water mixture, we would like to reiterate that the observed dynamics in this system is not the only way a system of coupled vibrations can behave. As earlier mentioned, if one substitutes the actual OH site frequencies with frequencies derived from a pure Gaussian process (modeled by the overdamped Brownian oscillator[3]), the dynamics of the symmetric/asymmetric modes becomes identical. Furthermore, even when the site frequencies exhibit non-Gaussian dynamics, the two eigenstates can behave identically if the site frequencies are perfectly correlated and/or the magnitude of the site frequency fluctuations is much smaller than the coupling. This can be directly seen from eq 1 from where the eigenfrequencies are derived as $\omega_{s,a}(t) = [\omega_1(t) + \omega_2(t)]/2 \pm J(t)$. If the coupling is weaker than the rms fluctuations of the site frequency (i.e., $\langle J(t) \rangle \ll (\langle \omega_1^2(t) \rangle - \langle \omega_1(t) \rangle^2)^{1/2}$), the two eigenfrequencies both behave in the same way as the site frequency, and the two eigenstates will exhibit identical dynamics. Finally, if the coupling is significantly correlated with the site frequencies and its fluctuations have a substantial magnitude, dissimilar dynamics of the eigenstates will be observed as well.

Conclusion

The dominant finding of this paper is undoubtedly the experimentally observed and theoretically verified difference in dynamics of the coupled vibrations. The way that non-Gaussian statistics together with the coupling affect symmetric and asymmetric mode dynamics could only be unraveled on the basis of combined quantum-mechanical and MD simulations. Furthermore, this is not exclusively restricted to coupled hydrogen-bonded systems but certainly applies to more general cases. Recently proposed 3D-IR spectroscopy[45] holds great promises for such studies.

References and Notes

(1) Jimenez, R.; Fleming, G. R.; Kumar, P. V.; Maroncelli, M. *Nature* **1994**, *369*, 471.
(2) Rossky, P. J.; Simon, J. D. *Nature* **1994**, *370*, 263.
(3) Mukamel, S. *Principles of Nonlinear Optical Spectroscopy*; Oxford University Press: New York, 1999.
(4) Brixner, T.; Stenger, J.; Vaswani, H. M.; Blankenship, R. E.; Fleming, G. R. *Nature* **2005**, *343*, 625.
(5) Demirdöven, N.; Cheatum, C. M.; Chung, H. S.; Khalil, M.; Knoester, J.; Tokmakoff, A. *J. Am. Chem. Soc.* **2004**, *126*, 7981.
(6) Jelley, E. E. *Nature* **1936**, *138*, 1009.
(7) Fidder, H.; Knoester, J.; Wiersma, D. A. *J. Chem. Phys.* **1991**, *95*, 7880.
(8) Heijs, D. J.; Malyshev, V. A.; Knoester, J. *J. Chem. Phys.* **2004**, *121*, 4884.
(9) Shortreed, M. R.; Swallen, S. F.; Shi, Z. Y.; Tan, W. H.; Xu, Z. F.; Devadoss, C.; Moore, J. S.; Kopelman, R. *J. Phys. Chem. B* **1997**, *101*, 6318.
(10) Barbour, L. W.; Hegadorn, M.; Asbury, J. B. *J. Am. Chem. Soc.* **2007**, *129*, 5884.
(11) Woutersen, S.; Bakker, H. J. *Nature* **1999**, *402*, 507.
(12) Tokmakoff, A. *Science* **2007**, *317*, 54.
(13) Torii, H. *J. Phys. Chem. A* **2006**, *110*, 9469.
(14) Cowan, M. L.; Bruner, B. D.; Huse, N.; Dwyer, J. R.; Chugh, B.; Nibbering, E. T. J.; Elsaesser, T.; Miller, R. J. D. *Nature* **2005**, *434*, 199.
(15) Kubo, R. *J. Phys. Soc. Jpn.* **1962**, *17*, 1100.
(16) Demirdöven, N.; Khalil, M.; Tokmakoff, A. *Phys. Rev. Lett.* **2002**, *89*, 237401.
(17) Davydov, A. S. *Solitons in molecular systems*; Reidel: Dordrecht, 1985.
(18) Anderson, P. W. *J. Phys. Soc. Jpn.* **1954**, *9*, 316.
(19) Hamm, P.; Lim, M. H.; Hochstrasser, R. M. *J. Phys. Chem. B* **1998**, *102*, 6123.
(20) Mukamel, S. *Annu. Rev. Phys. Chem.* **2000**, *51*, 691.
(21) Khalil, M.; Demirdoven, N.; Tokmakoff, A. *J. Phys. Chem. A* **2003**, *107*, 5258.
(22) Jonas, D. M. *Annu. Rev. Phys. Chem.* **2003**, *54*, 425.
(23) Golonzka, O.; Khalil, M.; Demirdöven, N.; Tokmakoff, A. *Phys. Rev. Lett.* **2001**, *86*, 2154.
(24) Lazonder, K.; Pshenichnikov, M. S.; Wiersma, D. A. *Opt. Lett.* **2006**, *31*, 3354.
(25) Thouless, J. D. *Phys. Rep.* **1974**, *13*, 93.

(26) Cringus, D.; Jansen, T. l. C.; Pshenichnikov, M. S.; Wiersma, D. A. *J. Chem. Phys.* **2007**, *127*, 084507.
(27) Kraemer, D.; Cowan, M. L.; Paarmann, A.; Huse, N.; Nibbering, E. T. J.; Elsaesser, T.; Miller, R. J. D. *Proc. Natl. Acad. Sci. U.S.A.* **2008**, *105*, 437.
(28) Kwak, K.; Rosenfeld, D. E.; Fayer, M. D. *J. Chem. Phys.* **2008,** *128,* 204505.
(29) Berendsen, H. J. C.; van der Spoel, D.; van Drunen, R. *Comput. Phys. Commun.* **1995**, *91*, 43.
(30) Guardia, E.; Pinzon, R.; Casulleras, J.; Orozco, M.; Luque, F. *J. Mol. Simul.* **2001**, *26*, 287.
(31) Berendsen, H. J. C.; Grigera, J. R.; Straatsma, T. P. *J. Phys. Chem. A* **1987**, *91*, 6269.
(32) Auer, B. M.; Skinner, J. L. *J. Chem. Phys.* **2007**, *127*, 104105.
(33) Schmidt, J. R.; Roberts, S. T.; Loparo, J. J.; Tokmakoff, A.; Fayer, M. D.; Skinner, J. L. *Chem. Phys.* **2007**, *341*, 143.
(34) Auer, B. M.; Skinner, J. L. *J. Chem. Phys.* **2008**, *128*, 224511.
(35) Jansen, T. l. C.; Knoester, J. *J. Phys. Chem. B.* **2006**, *110*, 22910.
(36) Jansen, T. l. C.; Knoester, J. *J. Chem. Phys.* **2007**, *127*, 234502.
(37) Khalil, M.; Demirdöven, N.; Tokmakoff, A. *J. Chem. Phys.* **2004**, *121*, 362.
(38) Venables, D. S.; Schmuttenmaer, C. A. *J. Chem. Phys.* **2000**, *113*, 11222.
(39) Fecko, C. J.; Eaves, J. D.; Loparo, J. J.; Tokmakoff, A.; Geissler, P. L. *Science* **2003**, *301*, 1698.
(40) Corcelli, S. A.; Lawrence, C. P.; Skinner, J. L. *J. Chem. Phys.* **2004**, *120*, 8107.
(41) de Boeij, W. P.; Pshenichnikov, M. S.; Wiersma, D. A. *J. Phys. Chem.* **1996**, *100*, 11806.
(42) Nee, M. J.; Baiz, C. R.; Anna, J. M.; McCanne, R.; Kubarych, K. J. *J. Chem. Phys.* **2008**, *129*, 084503.
(43) Nemeth, A.; Milota, F.; Mancal, T.; Lukeš, V.; Kauffmann, H. F.; Sperling, J. *Chem. Phys. Lett.* **2008**, *459*, 94.
(44) Møller, K. B.; Rey, R.; Hynes, J. T. *J. Phys. Chem. A* **2004**, *108*, 1275.
(45) Garret-Roe, S.; Hamm, P. *J. Chem. Phys.* **2008**, *128*, 104508.

JP900480R